



Generalization of the binary structural phase field crystal model

Nathan Smith and Nikolas Provatas

Department of Physics, McGill University, Montreal, Quebec, Canada H3A 0G4

(Received 28 August 2017; published 31 October 2017)

Two improvements to the binary structural phase field crystal (XPFC) theory are presented. The first is an improvement to the phenomenology for modelling density-density correlation functions and the second extends the free energy of the mixing term in the binary XPFC model beyond ideal mixing to a regular solution model. These improvements are applied to study kinetics of precipitation from solution. We observe a two-step nucleation pathway similar to recent experimental work [N. D. Loh, S. Sen, M. Bosman, S. F. Tan, J. Zhong, C. A. Nijhuis, P. Král, P. Matsudaira, and U. Mirsaidov, *Nat. Chem.* **9**, 77 (2017); A. F. Wallace, L. O. Hedges, A. Fernandez-Martinez, P. Raiteri, J. D. Gale, G. A. Waychunas, S. Whitlam, J. F. Banfield, and J. J. De Yoreo, *Science* **341**, 885 (2013)] in which the liquid solution first decomposes into solute-poor and solute-rich regions, followed by precipitate nucleation of the solute-rich regions. Additionally, we find a phenomenon not previously described in the literature in which the growth of precipitates is accelerated in the presence of uncrystallized solute-rich liquid regions.

DOI: [10.1103/PhysRevMaterials.1.053407](https://doi.org/10.1103/PhysRevMaterials.1.053407)

I. INTRODUCTION

The study of alloys in materials physics is a pursuit of incredibly broad impact, affecting industries as diverse as those dealing with commercial materials such as steel and aluminium alloys to nanofabrication and optoelectronics. Understanding of alloy properties can be difficult due to their strong dependence on microstructure which forms through nonequilibrium processes during their manufacturing. *In situ* measurements of microstructure formation, especially at the atomic level, are rarely feasible.

A broad spectrum of theoretical and numerical techniques has been successful at predicting microstructure formation. In particular, the phase field crystal (PFC) technique has been successful in describing microstructure at diffusive time scales and atomic length scales at high temperatures where other techniques including kinetic Monte Carlo, diffusive molecular dynamics, and accelerated molecular dynamics can fail.

In this paper, we focus on extending a branch of binary PFC theory known as the binary structural phase field crystal (XPFC) model—where the X in XPFC signifies a class of PFC models constructed to controllably simulate a robust range of metallic and nonmetallic crystal symmetries compared to the original PFC models. PFC binary models have been successful in describing a broad selection of phenomena in binary alloys. These successes include eutectic and dendritic solidification [1], the Kirkendall effect [2,3], solute drag [4], clustering and precipitation [5–7], colloidal ordering in drying suspensions [8], epitaxial growth and island formation [9,10], and ordered crystals [11,12] to name a few.

The PFC theory is derived from classical density functional theory (CDFT) and, as such, it can be considered a simplified density functional theory. In a cruder sense, PFC theories can also be seen as phase field models containing an order parameter related to density that can attain periodic states. In practice, two different variants of the PFC theory have been extensively used to model binary alloys, as alluded to above: The original model developed by Elder *et al.* [1] and the XPFC model developed by Greenwood *et al.* [13].

The original model was the first PFC theory of binary alloys and contains several important physical properties of

binary alloys. However, it is a reduced form of CDFT and it therefore lacks completeness in its ability to describe binary alloys. Specifically, the original model uses an expansion in concentration that is actually a density difference, not a concentration, and the model has a limited ability to describe a realistic or robust range of phase diagrams. The original model also uses a very simplified correlation kernel which limits its ability to describe a variety of crystal lattice structures.

The binary XPFC model is an improvement that ameliorates the above problems. The concentration is left unexpanded, allowing for construction of realistic global phase diagrams instead of local expansions. More significantly, the XPFC model provides a phenomenology for modeling two-point correlation functions that succeeded in describing solidification of a variety of lattice structures, as well as transformations between different crystal lattices. Simplifications of the multimodal approach first introduced with the XPFC formalism have been used to produce hexagonal, square, kagome, honeycomb, rectangular, and other lattices in two dimensions [14].

In introducing its phenomenology for modeling correlation functions, the original binary XPFC theory tacitly assumes that there is some preferred structure at high concentration and some other structure preferred at low concentration. This assumption can be limiting in situations where a specific crystalline structure occurs at intermediate concentrations. An important example is that of materials with a syntectic reaction. At the syntectic point a solid of intermediate concentration solidifies along the interface between a solute-rich and solute-poor liquid. The binary XPFC model also assumes no long-wavelength correlations in the concentration field, which, in practice, means the model has an ideal free energy of mixing. This is another limitation of the XPFC model because the enthalpy of mixing is not generally zero for real alloy systems.

The goal of the current paper is threefold: The first two goals are to present two important improvements to the binary XPFC theory. The first improvement is a more general phenomenology for modeling pair-correlation functions of a binary material. The second improvement is to extend the free energy of mixing beyond ideality to account for circumstances

when the enthalpy of mixing is not negligible. The third goal is to use the XPFC model derived herein to elucidate the multistep nucleation process observed in certain diffusion-limited systems precipitating gold and silver nanoparticles from solution [15].

II. BINARY CDFT

We begin with a classical density functional theory for binary systems. The intrinsic free-energy functional can be approximated by expanding about a reference mixture state with number densities ρ_A^0 for component A and ρ_B^0 for component B:

$$\begin{aligned} \beta\mathcal{F}[\rho_A, \rho_B] &= \sum_i \int dr \left\{ \rho_i(r) \ln \left(\frac{\rho_i(r)}{\rho_i^0} \right) - (1 - \beta\mu_i^0) \Delta\rho_i(r) \right\} \\ &\quad - \frac{1}{2} \sum_{i,j} \Delta\rho_i(r) * C_{ij}^{(2)}(r, r') * \Delta\rho_j(r'), \end{aligned} \quad (1)$$

where the sums run over components A and B, μ_i^0 is the reference chemical potential of component i , $\Delta\rho_i$ is the deviation from the reference density of component i , $C_{ij}^{(2)}(r, r')$ is the direct correlation function of the reference mixture, and $*$ denotes an integral over repeated arguments, i.e.,

$$f(r) * g(r) \equiv \int dr f(r) g(r) \quad (2)$$

and $\beta = 1/k_B T$ where T is temperature and k_B is Boltzmann's constant. It is convenient to change variables to a dimensionless total density $n(r)$ and local concentration $c(r)$:

$$n(r) = \frac{\Delta\rho}{\rho_0} = \frac{\Delta\rho_A + \Delta\rho_B}{\rho_A^0 + \rho_B^0}, \quad (3)$$

$$c(r) = \frac{\rho_B}{\rho} = \frac{\rho_B}{\rho_A + \rho_B}. \quad (4)$$

Scaling out a factor of the total reference density, ρ_0 , we can break the free-energy functional in these new variables into three parts:

$$\frac{\beta\mathcal{F}[n, c]}{\rho_0} = \frac{\beta\mathcal{F}_{\text{id}}[n]}{\rho_0} + \frac{\beta\mathcal{F}_{\text{mix}}[n, c]}{\rho_0} + \frac{\beta\mathcal{F}_{\text{ex}}[n, c]}{\rho_0}, \quad (5)$$

where \mathcal{F}_{id} , \mathcal{F}_{mix} , and \mathcal{F}_{ex} are the ideal, mixing, and excess free energies, respectively. These are defined as

$$\frac{\beta\mathcal{F}_{\text{id}}}{\rho_0} = \int dr \{ [n(r) + 1] \ln [n(r) + 1] - (1 - \beta\mu^0) n(r) \} \quad (6)$$

and

$$\begin{aligned} \frac{\beta\mathcal{F}_{\text{mix}}}{\rho_0} &= \int dr \left\{ [n(r) + 1] \right. \\ &\quad \left. \times \left[c \ln \left(\frac{c}{c_0} \right) + (1 - c) \ln \left(\frac{1 - c}{1 - c_0} \right) \right] \right\}, \end{aligned} \quad (7)$$

where we have introduced $\mu^0 = \mu_A^0 + \mu_B^0$ as the total chemical potential of the reference mixture and $c_0 = \rho_B^0/\rho_0$ as the reference concentration. Assuming that the local concentration

$c(r)$ varies over much longer length scales than the local density $n(r)$, the excess free-energy term becomes

$$\begin{aligned} \frac{\beta\mathcal{F}_{\text{ex}}[n, c]}{\rho_0} &= -\frac{1}{2} \{ n(r) * C_{nn}(r, r') * n(r') \\ &\quad + n(r) * C_{nc}(r, r') * \Delta c(r') \\ &\quad + \Delta c(r) * C_{cn}(r, r') * n(r') \\ &\quad + \Delta c(r) * C_{cc}(r, r') * \Delta c(r') \}, \end{aligned} \quad (8)$$

where we have introduced $\Delta c(r) = c(r) - c_0$ as the deviation of the concentration from the reference. The four n - c pair-correlation functions introduced in the excess free energy are given by

$$C_{nn} = \rho_0 [c^2 C_{BB} + (1 - c)^2 C_{AA} + 2c(1 - c) C_{AB}], \quad (9)$$

$$C_{nc} = \rho_0 [c C_{BB} - (1 - c) C_{AA} + (1 - 2c) C_{AB}], \quad (10)$$

$$C_{cn} = C_{nc}, \quad (11)$$

$$C_{cc} = \rho_0 (C_{BB} + C_{AA} - 2C_{AB}). \quad (12)$$

Differences in the various binary PFC theories stem from differing approximations of the terms in the free energy stated in Eqs. (6)–(8). These are discussed briefly next. Further details of the derivations leading to the above equations, and those discussed below, are found in Ref. [16].

III. ORIGINAL BINARY PFC MODEL

In the original simplified binary PFC theory of Ref. [1], all terms in the free energy are expanded about $n(r) = 0$ and $c(r) = c_0$, i.e., about their reference states. For the ideal free energy this results in a polynomial truncated to fourth order:

$$\frac{\beta\mathcal{F}_{\text{id}}[n]}{\rho_0} = \int dr \left\{ \frac{n(r)^2}{2} - \eta \frac{n(r)^3}{6} + \chi \frac{n(r)^4}{12} \right\}. \quad (13)$$

The linear term in the expansion is dropped by redefining n about its average and we have added the fitting parameters η and χ to fit the free energy away from the reference parameters. If we assume for simplicity of demonstration $c_0 = 1/2$, the free energy of mixing becomes a simple fourth-order polynomial as well:

$$\frac{\beta\mathcal{F}_{\text{mix}}[n, c]}{\rho_0} = \int dr \left\{ 2\Delta c(r)^2 + \frac{4\Delta c(r)^4}{3} \right\}. \quad (14)$$

The linear couplings to $n(r)$ are dropped in this expansion by assuming, as we already have, that the concentration field varies on a much longer length scale than the total density and noting that the total density is defined about its average. This argument can also be applied to the linear couplings to $n(r)$ in the excess free-energy term, which then leaves only the C_{nn} and C_{cc} terms. These two terms are approximated with a gradient expansion of the form

$$C_{nn}(r, r') = (C_0 + C_2 \nabla^2 + C_4 \nabla^4 + \dots) \delta(r - r'), \quad (15)$$

$$C_{cc}(r, r') = (\epsilon + W_c \nabla^2 + \dots) \delta(r - r'). \quad (16)$$

The expansion parameters C_0, C_2 , and C_4 are all dependent on temperature and concentration. We are required to expand C_{nn} to fourth order because the peak of the direct correlation function in Fourier space is the driving force for solidification. The concentration field is correlated over a longer length scale implying that only the short wave vectors are important in C_{cc} so we can expand just to quadratic order, effectively treating c as in the traditional Cahn-Hilliard theory.

Gathering terms, the resulting free-energy functional for the original simplified binary PFC model [17] is

$$\frac{\beta\mathcal{F}}{\rho_0} = \int dr \left\{ \frac{1}{2}n(1 - C_0 - C_2\nabla^2 - C_4\nabla^4)n - \eta\frac{n^3}{6} + \chi\frac{n^4}{12} + \frac{1}{2}\Delta c(4 - \epsilon - W_c\nabla^2)\Delta c + \frac{4\Delta c^4}{3} \right\}. \quad (17)$$

The strength of the original simplified binary PFC model is that it retains most of the important physics of binary alloys in a very reduced theory. For instance, this model is capable of describing the equilibrium phase diagrams of both eutectic alloys and materials with a solid-state spinodal or liquid minimum. Supplied with a diffusive equation of motion, this model can simulate an impressive diversity of dynamic phenomena including eutectic growth [1], solute segregation [18], dendritic growth [1], epitaxial growth [9,10], and crack formation [19].

The major limitation of the original simplified model is that the gradient expansion of the density-density correlation function gives only a crude control over the crystal structures that can be formed. In fact, as this theory only controls a single peak in Fourier space it can only solidify into a body centered cubic (bcc) phase.

A second limitation of the original simplified model is that it is local in concentration. This means that realistic phase diagrams from 0 to 100% concentration cannot be produced, only local phase diagrams around the reference concentration [20]. The limited concentration range is problematic for comparing to experimental phase diagrams. To obtain reliable and quantitative results—a major motivation for the original binary XPFC model and the model in this paper—we require the entire free energy of the mixing term in Eq. (7).

IV. ORIGINAL BINARY XPFC MODEL

In the original binary XPFC model seeks to remedy the two shortcomings of the original simplified binary PFC model. That is, it seeks to reproduce a variety of crystal lattice structures and to construct phase diagrams of a complete range of concentrations. We derive this theory here and compare it with the original model.

First, the ideal free energy is expanded in precisely the same manner as before, resulting in the same fourth-order polynomial:

$$\frac{\beta\mathcal{F}_{id}[n]}{\rho_0} = \int dr \left\{ \frac{n(r)^2}{2} - \eta\frac{n(r)^3}{6} + \chi\frac{n(r)^4}{12} \right\}. \quad (18)$$

The free energy of mixing is left unexpanded but an overall scale ω is added to help modify the mixing term away from

the reference concentration:

$$\frac{\beta\mathcal{F}_{mix}[n,c]}{\rho_0} = \int dr \left\{ \omega[n(r) + 1] \times \left[c \ln\left(\frac{c}{c_0}\right) + (1-c) \ln\left(\frac{1-c}{1-c_0}\right) \right] \right\}. \quad (19)$$

This unexpanded free energy of mixing will lead to more accurate global phase diagrams. The excess free energy is approximated using similar assumptions as in the original binary PFC model (linear couplings are dropped), but the density-density correlation function, C_{nn} , is not expanded. Also, Greenwood *et al.* [13] all assumed that the $k = 0$ mode of the concentration-concentration correlation function is zero, leaving only the quadratic term in the expansion:

$$C_{cc}(r,r') = \delta(r-r')W_c\nabla^2. \quad (20)$$

Grouping terms together, the complete free-energy functional for the original binary XPFC model is

$$\frac{\beta\mathcal{F}}{\rho_0} = \int dr \left\{ \frac{1}{2}n(r)[1 - C_{nn}(r,r')] * n(r') - \eta\frac{n^3}{6} + \chi\frac{n^4}{12} + \frac{W_c}{2}|\nabla c(r)|^2 + \omega f_{mix}(r) \right\}, \quad (21)$$

where $f_{mix}(r)$ is the local free-energy density of mixing:

$$f_{mix}(r) = [n(r) + 1] \left[c(r) \ln\left(\frac{c(r)}{c_0}\right) + [1 - c(r)] \ln\left(\frac{1-c(r)}{1-c_0}\right) \right]. \quad (22)$$

The density-density correlation function, C_{nn} , is left unexpanded in Fourier space but assumed to have a specific phenomenological real-space form:

$$C_{nn} = \zeta_A(c)C_{AA}(r,r') + \zeta_B(c)C_{BB}(r,r'), \quad (23)$$

where $\zeta_A(c)$ and $\zeta_B(c)$ are interpolation functions, assigned the forms

$$\zeta_A(c) = 1 - 3c^2 + 2c^3, \quad (24)$$

$$\zeta_B(c) = \zeta_A(1-c) \quad (25)$$

by Greenwood *et al.* [13].

The remaining elemental correlation functions C_{AA} and C_{BB} are modeled using the form of the two-point correlations in the original XPFC model for a pure material introduced by Greenwood *et al.* [21]. This is described subsequently.

A. XPFC correlation functions

The main contribution of the XPFC model is that the density-density correlation function can be modeled in such a way as to control the crystal lattice structure formed under solidification and to target different structures at different concentrations and temperatures. Originally delineated for pure systems, the XPFC method introduces a model correlation function with controllable height and reciprocal-lattice vector position for each family of correlation peaks. This is achieved

by using Gaussian peaks centered at the reciprocal-lattice vector positions:

$$\tilde{C}(k) = \sum_{\alpha} e^{-\frac{T}{T_0}} e^{-\frac{(k-k_{\alpha})^2}{2\sigma_{\alpha}^2}} \quad (26)$$

where the index α runs over sets of point-group symmetry-equivalent reciprocal-lattice vectors, k_{α} is the length of the reciprocal-lattice vectors in α , and σ_{α} is the width of the peak. Following Ref. [12], temperature dependence of the correlation peaks is achieved through the prefactors e^{-T/T_0} , which give the correct temperature scaling of the amplitudes at temperatures much higher than the Debye temperature [22].

The primary advantages of the XPFC model are twofold: They produce realistic phase diagrams and they model a variety of crystalline lattices. The latter is particularly significant as it allows for the examination of genuinely novel systems in comparison with the original simplified model. For example, the binary XPFC model has been used to study peritectic systems [13], ordered crystals [12], dislocation-assisted solute clustering and precipitation [5,6], and solute drag [4]. It is noteworthy that the above works on clustering have been validated experimentally in binary and ternary alloys.

Unfortunately, by assuming that the $k = 0$ mode of the concentration-concentration correlation function is zero, the XPFC model restricts its free energy of mixing to an ideal model of mixing. This model of mixing includes only entropic contributions to the free energy. In the solid state, this means that the sole driving force for phase separation is elastic energy, as the enthalpy of mixing is always zero. This inhibits the modeling of a variety of binary alloy systems; for instance, both monotectic and syntectic systems cannot be modeled without a negative enthalpy of mixing.

A second disadvantage of the present XPFC model is that the phenomenological form for the correlation function given by Eqs. (23)–(25) implicitly assumes that there are well-defined structures at $c = 0$ and 1. This works well for modeling eutectic systems, but does not work very well when we expect a solid phase at intermediate concentration. These shortcomings are the motivation for the improvements developed in this paper, which are presented in the following section.

V. GENERALIZATION OF THE BINARY STRUCTURAL PHASE FIELD CRYSTAL MODEL

In this section we look at two improvements to the binary XPFC theory. The improvements, as previously alluded to, are first to extend the free energy of mixing in the XPFC model to one with an enthalpy of mixing, and second to generalize the phenomenological form of the two-point correlation function in binary alloys.

A. Adding an enthalpy of mixing

Extending the free energy of mixing beyond ideal mixing is achieved by removing the assumption made by Greenwood *et al.* [13] in deriving the binary XPFC model that the concentration-concentration correlation function has no $k = 0$ mode. This is the same approach taken in the original PFC model, though here we keep the ideal mixing term

unexpanded as in the original XPFC alloy model. Specifically, the correlation function is expanded as

$$C_{cc}(r, r') = \delta(r - r')(\omega\epsilon + W_c\nabla^2 + \dots), \quad (27)$$

where ϵ is a parameter that is possibly temperature dependent. This form results in a free-energy functional of the form

$$\frac{\beta\mathcal{F}}{\rho_0} = \int dr \left\{ \frac{1}{2}n(r)[1 - C_{nn}(r, r')] * n(r') - \eta\frac{n^3}{6} + \chi\frac{n^4}{12} + \frac{W_c}{2}|\nabla c(r)|^2 + \omega f_{\text{mix}}(r) \right\}, \quad (28)$$

where the local free-energy density of mixing, f_{mix} , is now

$$f_{\text{mix}}(r) = [n(r) + 1] \left[c(r) \ln \left(\frac{c(r)}{c_0} \right) + [1 - c(r)] \ln \left(\frac{1 - c(r)}{1 - c_0} \right) \right] + \frac{1}{2}\epsilon(c - c_0)^2. \quad (29)$$

For simplicity the temperature dependence of the parameter ϵ is taken to be linear about a spinodal temperature T_c :

$$\epsilon(T) = -4 + \epsilon_0(T - T_c). \quad (30)$$

The resulting model has a free energy of mixing that is equivalent to the regular solution model and, as such, it makes a clear connection to other well-known models used elsewhere in material science. The regular solution model also supplies the essential physics of a non-negligible enthalpy of mixing.

B. Generalizing the two-point correlation function

To establish a general phenomenology for modeling density-density correlation functions in alloys, we consider a density-density correlation function that has the form of a linear combination of general interpolating functions in concentration, $\zeta(c)$, multiplied by bare correlation functions $C(r, r')$ of individual components:

$$C_{nn}(r, r'; c) = \sum_i \zeta_i(c) C_i(r, r') \quad (31)$$

where the index i is, for the moment, an arbitrary label. For example, in the exact theory that emerges from the original alloy CDFT theory [Eq. (9)], we use the labels $i \in \{AA, AB, BB\}$ to enumerate the three interpolation functions:

$$\zeta_{AA}(c) = \rho_0(1 - c^2), \quad (32)$$

$$\zeta_{AB}(c) = \rho_0 c(1 - c), \quad (33)$$

$$\zeta_{BB}(c) = \rho_0 c^2. \quad (34)$$

This suggests the following definition that we introduce herein to generalize the density-density correlation function for a binary alloy. Use the labels i to enumerate the set of crystal structures known to manifest themselves in an alloy system. The correlation functions, $C_i(r, r')$, are then direct correlation functions that model the formation of the crystal structure i , and the associated interpolation functions $\zeta_i(c)$ define the range of concentrations over which these correlations are valid. In principle, $\zeta_i(c)$ can also be temperature dependent, although we do not consider that case in this paper.

As a simple example, if we wanted to construct a model of the silver-copper eutectic alloy system, we might start with some model correlation function for pure silver, $C_\alpha(r, r')$, and for pure copper, $C_\beta(r, r')$. These two structures, the silver-rich α phase and the copper-rich β phase, are the only two relevant crystalline phases in this system; thus, to build the full density-density correlation function we just need to choose interpolating functions for each phase. Following Greenwood *et al.* [13], for example, we might choose

$$\zeta_\alpha(c) = 1 - 3c^2 + 2c^3, \quad (35)$$

$$\zeta_\beta(c) = 1 - 3(1 - c)^2 + 2(1 - c)^3. \quad (36)$$

To model the α and β correlation functions we use the original XPFC formalism for modeling bare correlation functions, i.e., Eq. (26). The α and β phase are both fcc [23] so we can use a two-peak fcc model for the correlation function as in Ref. [21].

VI. EQUILIBRIUM PROPERTIES OF BINARY ALLOYS

These two changes to the XPFC formalism extend the possible systems we can study. In this section we explore the equilibrium properties of the improved XPFC free-energy functional specialized for three different material phase diagrams: eutectic, syntectic, and monotectic.

A. Eutectic phase diagram

While previous PFC models have shown that elastic energy is a sufficient driving force for eutectic solidification, our simplified regular solution XPFC model allows for the examination of the role enthalpy of mixing can play in eutectic solids. For instance, Murdoch and Schuh noted that in nanocrystalline binary alloys, while a positive enthalpy of segregation can stabilize against grain growth via solute segregation at the grain boundary, if the enthalpy of mixing becomes too large this effect can be negated by second phase formation or even macroscopic phase separation [24].

To specialize our simplified regular solution model to the case of the binary eutectic, we must choose an appropriate model for the correlation function. Choosing an α phase around $c = 0$ and β phase around $c = 1$, we can recover the pair-correlation function used in the binary XPFC of Greenwood *et al.* [13] with a particular choice of interpolations functions:

$$\zeta_\alpha(c) = 2c^3 - 3c^2 + 1, \quad (37)$$

$$\zeta_\beta(c) = \zeta_\alpha(1 - c). \quad (38)$$

Choosing, for example, an α and β phase with two-dimensional hexagonal lattices, differing only by lattice constants, we can produce a phase diagram like that in Fig. 1. The figure also depicts the phase diagram of the metastable liquid below the eutectic point showing the binodal and spinodal lines where the metastable liquid becomes unstable with respect to phase separation. The spinodal line indicates an inflexion point in the free energy of the metastable liquid where the liquid becomes fully unstable with respect to phase separation whereas the binodal line indicates the coexistence curve of the decomposed metastable liquid.

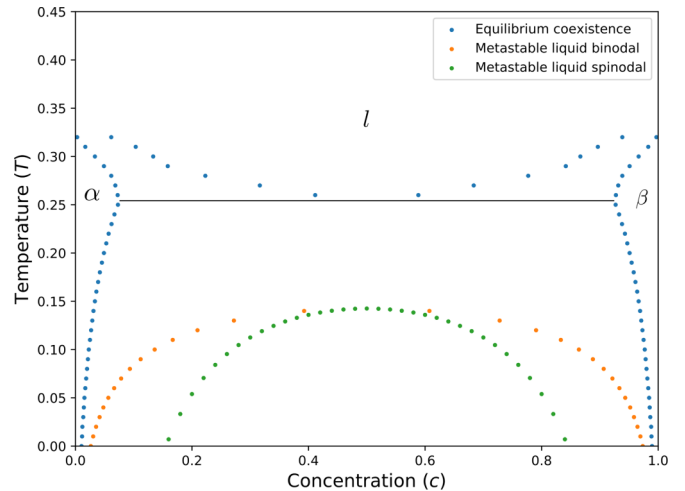


FIG. 1. Eutectic phase diagram for triangular α and β solid phases, and l denotes the liquid. The free-energy parameters are $\eta = 2$, $\chi = 1$, $\omega = 0.02$, $\epsilon_0 = 26.6$, and $T_c = 0.15$. The parameters of the correlation functions are $\sigma_{10\alpha} = \sigma_{10\beta} = 0.8$, $k_{10\alpha} = 2\pi$, $k_{10\beta} = 4\pi/\sqrt{3}$, and $T_0 = 1$. The horizontal line denotes the eutectic temperature.

It is noted that the phase diagram in Fig. 1 and in what follows were done using the same approach that was used in numerous PFC literature [13]. The approach is as follows: A mode expansion for the density is assumed for each crystal phase (zero amplitudes for the liquid phase). For each phase, a free energy results, which is a function of amplitudes, average density, and concentration. This coarse grained free energy of each phase is then minimized with respect to the amplitudes, leaving a free-energy density for each phase that is a function only of the average density and concentration. At this juncture, we simplify matters by assuming that the average density is a constant for the system. We then minimize the total free energy of the system with respect to concentration, assuming a conserved total concentration field. This latter step considers separately the coexistence of (1) α -liquid, (2) β -liquid, and (3) α - β solids over different temperature and concentration ranges. An original code was developed to carry out these phase diagram constructions, and implemented using JULIA [25], MAXIMA.JL [26], and the MAXIMA symbolic computation engine [27].

B. Syntectic phase diagram

Our improved XPFC model also allows for the study of a variety of invariant binary reactions that, to date, have not been studied using phase field crystal models. One such reaction is the syntectic reaction.

The syntectic reaction, $l_1 + l_2 \rightarrow \alpha$, consists of solidification at the interface of two liquids. We can achieve this with our model by setting the spinodal temperature, T_c , in Eq. (30) sufficiently high and producing a density-density correlation function that is peaked at a concentration below the spinodal. This can be done by choosing a single interpolation function to be a window function that is centered about an intermediate concentration c_α of the solid phase α . One obvious choice is

$$\zeta(c) = e^{-\frac{(c-c_\alpha)^2}{2\alpha^2}} \quad (39)$$

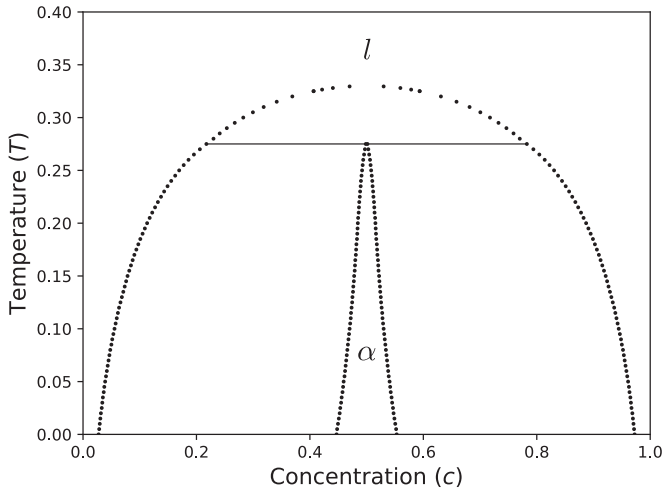


FIG. 2. Phase diagram of a syntectic alloy with a hexagonal solid phase α . The free-energy parameters are $\eta = 2$, $\chi = 1$, $\omega = 0.3$, $\epsilon_0 = 10$, $T_c = 0.35$, and $c_0 = 0.5$. The parameters for the correlation function are $\alpha_{10\alpha} = 0.8$, $k_{10\alpha} = 2\pi$, and $T_0 = 1$ and the parameters for the window function are $c_{10\alpha} = 0.5$ and $\alpha_c = 0.5$. The horizontal line denotes the syntectic temperature.

where α_c is a constant. The resulting correlation function for a hexagonal lattice in a syntectic alloy in two dimensions becomes

$$\tilde{C}_{nm}(k; c) = e^{-\frac{(c-c_0)^2}{2\alpha_c^2}} e^{-\frac{T}{T_0}} e^{-\frac{(k-k_0)^2}{2\alpha^2}}, \quad (40)$$

where we have written the correlation function in Fourier space and α is the width of the peak corresponding to k_α . A phase diagram that produces a syntectic reaction with an appropriate choice of parameters is shown in Fig. 2.

C. Monotectic phase diagram

The monotectic reaction is another invariant binary reaction that has not previously been studied using PFC models. The monotectic reaction, $l_1 \rightarrow \alpha + l_2$, consists of decomposing liquid into a solute-poor solid and solute-rich liquid. To model a monotectic using our XPFC model we hypothesize a solid phase at $c = 0$ and set the spinodal temperature higher than the solidification temperature. To achieve this, we use a window function peaked around $c = 0$:

$$\chi_\alpha(c) = e^{-\frac{c^2}{2\alpha_c^2}}. \quad (41)$$

Again considering a simple hexagonal lattice for the α phase, we can produce a phase diagram with a monotectic reaction with an appropriate choice of parameters as shown in Fig. 3.

The improvements to the XPFC formalism made in this section can be used not only to reveal new details in existing systems but also to model new systems that have not been explored with PFC methods before. They provide a general framework to explore the landscape of other possible binary alloys with an emphasis that the liquid free energy is a crucial element in a complete description. It is also noteworthy that the approach introduced here is extendable in a straightforward way to multicomponent alloys if the interpolation functions become multivariate functions of the concentrations.

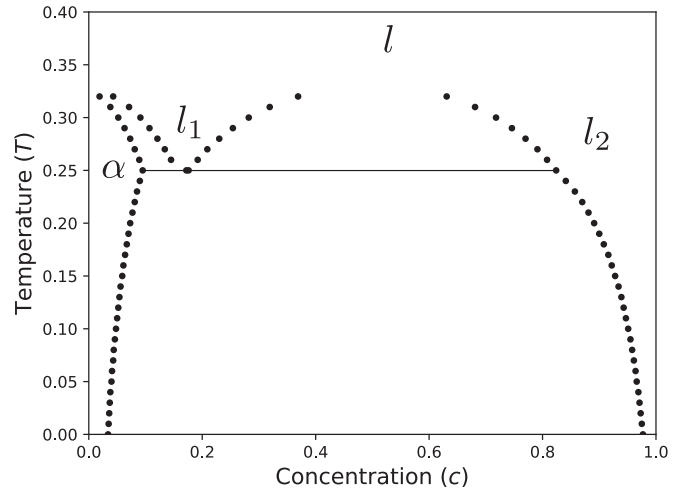


FIG. 3. Phase diagram of a monotectic alloy with hexagonal α phase. The free-energy parameters are $\eta = 2$, $\chi = 1$, $\omega = 0.3$, $\epsilon_0 = 10$, $T_c = 0.35$, and $c_0 = 0.75$. The parameters for the correlation function are $\alpha_{10\alpha} = 0.8$, $k_{10\alpha} = 2\pi$, and $T_0 = 1$ and the parameter for the window function is $\alpha_c = 0.4$. The horizontal line indicates the monotectic temperature.

VII. APPLICATION TO PRECIPITATING NANOPARTICLES FROM SOLUTION

In this section we discuss an application of the binary XPFC model introduced in Sec. V to a phenomenon in microstructure evolution. To begin with, we first introduce a phenomenological set of equations of motion that describe solute and density diffusion in the binary XPFC model. We then apply these to the examination of the process of diffusion limited precipitation from solution. Recent experimental work on the precipitation of gold and silver nanoparticles [15] and on the precipitation of calcium carbonate [28] has demonstrated that the pathway to nucleation can deviate highly from the approximations of classical nucleation theory (CNT). Specifically, experiments in both systems observe spinodal decomposition of the solution prior to nucleation in the solute-rich phase. In this section, we present early findings from our model that lend support for this dynamical behavior and, additionally, show that the growth behavior postnucleation may be more complex than usual diffusive growth and coarsening typically observed. To conclude we discuss future applications both in the study of precipitation and other areas.

A. XPFC dynamics

To examine applications of our improvements to the XPFC model we begin by considering equations of motion. Following Ref. [13], we use conservative dynamics for both $n(x, t)$ and $c(x, t)$:

$$\frac{\partial n(x, t)}{\partial t} = M_n \nabla^2 \left(\frac{\delta \beta \Delta \mathcal{F} / \rho_0}{\delta n(x, t)} \right) + \xi_n(x, t), \quad (42)$$

$$\frac{\partial c(x, t)}{\partial t} = M_c \nabla^2 \left(\frac{\delta \beta \Delta \mathcal{F} / \rho_0}{\delta c(x, t)} \right) + \xi_c(x, t), \quad (43)$$

where M_n and M_c are the solute and density mobilities. The noise terms $\xi_n(x, t)$ and $\xi_c(x, t)$ model thermal fluctuations by obeying a generalized Einstein relation [16]. These equations

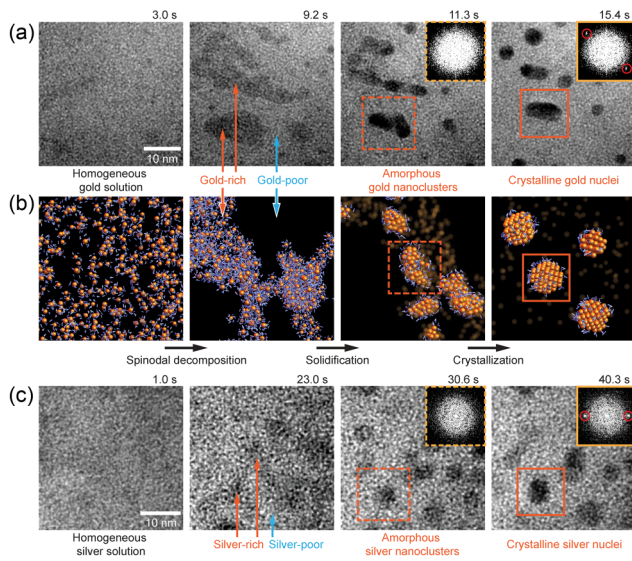


FIG. 4. Experimental observations of multistep nucleation and proposed three-step pathway due to Loh *et al.* [15]. Series (a) and (c) show TEM images of supersaturated gold and silver aqueous solutions precipitating. Series (b) shows a schematic of the proposed mechanism. Figure reused with explicit permission from the author.

of motion are largely phenomenological as, strictly speaking, there is no reason that the local concentration should be conserved. This conservation can be justified in the limit that the total density does not deviate far from the reference. When this is the case we have $c \equiv \rho_B/\rho \approx \rho_B/\rho_0$, which is conserved. For simplicity, we will carry out simulations in this paper in this limit.

B. Multistep nucleation of nanoparticles in solution

Many nanoparticle solutions are formed by precipitation from solution and their size distribution (polydispersity index) is of key importance to their application. Therefore, a precise understanding of the kinetic pathway of precipitation is of crucial importance in designing synthesis techniques of highly monodisperse nanoparticles.

As stated above, recent experimental work has shown that precipitation from a solution can follow a pathway that is very different from that assumed by CNT [15,28]. CNT assumes that, for binary systems, changes in composition occur simultaneously to changes in order. In contrast, these experimental findings suggest that in certain systems changes in composition can precede changes in order via spinodal decomposition. *In situ* measurements of this multistep nucleation process taken by Loh *et al.* [15] for gold and silver nanoparticles can be seen in Fig. 4. While there is some dispute about whether or not to call this process a nonclassical *nucleation* pathway [29,30], the observed pathway to precipitation raises several questions about its classification, regardless of semantics.

C. Classical and nonclassical nucleation theories

In CNT, the rate of formation of postcriticality can be written as an Arrhenius equation:

$$J = \frac{\partial n^*}{\partial t} = Ae^{-\beta\Delta G^\ddagger}, \quad (44)$$

where A is a constant prefactor, ΔG^\ddagger is the Gibbs free energy of a critical nucleus, and n^* is the number of critical nuclei.

Following Ref. [31], the probability of nucleation of a droplet of volume V , $f_{\text{nuc}}(t)$, is then

$$f_{\text{nuc}}(t) = \left\langle \frac{N_{\text{cry}}}{N_{\text{total}}} \right\rangle = 1 - e^{-JVt}, \quad (45)$$

where N_{cry} and N_{total} are the number of crystalline droplets and the total number of crystal droplet forming sites, respectively.

CNT assumes that there is a single critical state which is specified by the thermodynamic parameters of the target phase at a critical radius R^* . This naive approach dramatically underestimates the time required to assemble a critical nucleus due to its simplistic parametrization of the kinetic pathway [31–33].

Improvements to CNT can be made to the model by increasing the parameter space describing the nucleation process. Considering both radius and density of the critical nucleus [32] gives good agreement with nucleation of globular proteins, for example. One problem with this approach is the selection of appropriate parameters. There is no guarantee that a finite set of parameters will describe the kinetic pathway taken by a nucleus and if we are without a fundamental technique for calculating the chosen parameters we have little way of knowing if our theory is accurate or simply overfit. In Ref. [33], for example, nucleation data are fit to the functional form instead of using calculated or otherwise measured parameters.

Statistical field theories such as the XPFC alloy model can help provide an answer to this problem by taking an unbiased approach to the nucleation process within the context of CDFT, with thermal fluctuations. The critical state, and entire kinetic pathway, can be examined free of any particular path parametrization. The equations of motion can be integrated numerically for an ensemble of systems and nucleation details measured from the computed results. Moreover, unlike other numerical approaches to nucleation like molecular dynamics or formal density functional theory, the PFC model can examine nucleation on diffusive time scales.

D. XPFC modeling of precipitation

To construct an appropriate free-energy functional for a system analogous to gold nanoparticles studied by Loh *et al.* [15] we consider the structure of its equilibrium phase diagram. Precipitation is indicative of a simple liquid-solid coexistence curve. The presumed presence of spinodal decomposition under certain circumstances indicates that there is a metastable liquid spinodal submerged beneath the liquid-solid coexistence curve [29]. We assume that there must exist conditions under which the spinodal decomposition of the metastable liquid phase occurs more rapidly than nucleation directly from solution, i.e., classical nucleation.

Producing a phase diagram in our XPFC model with these characteristics is very similar to modeling a monotectic system with the exception that the spinodal temperature T_c must be low enough to hide the entire liquid spinodal below the coexistence curve. We will also center the interpolation function $\zeta_\alpha(c)$ about $c = 1$ so that the nanocrystalline solid α is favored at large concentration. The resulting density-density correlation

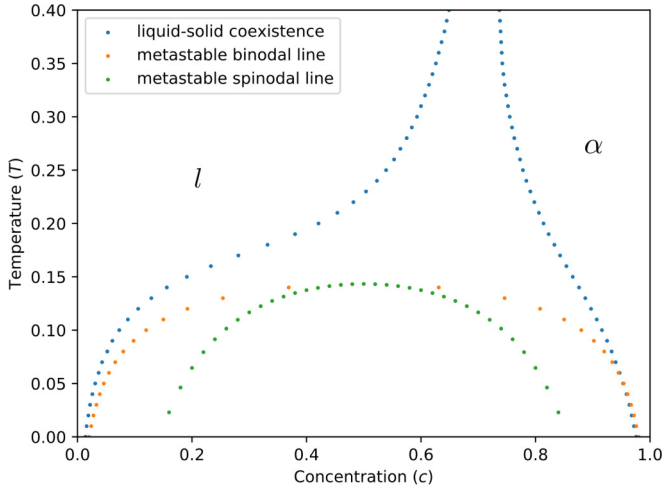


FIG. 5. Phase diagram of a precipitating solution with hexagonal α phase solid. The free-energy parameters are $\eta = 2$, $\chi = 1$, $\omega = 0.3$, $\epsilon_0 = 30$, $T_c = 0.15$, and $c_0 = 0.5$. The parameters for the correlation function from Eq. (46) are $\sigma = 0.8$, $k_{10} = 2\pi$, $T_0 = 1$, and $\sigma_c = 0.5$.

function for a two-dimensional hexagonal precipitate would thus be

$$\tilde{C}_{nn}(k; c) = e^{-\frac{(c-1)^2}{2\sigma_c^2}} e^{-\frac{T}{T_0}} e^{-\frac{(k-k_{10})^2}{2\sigma^2}}, \quad (46)$$

where σ_c is the width of the interpolation function $\zeta_\alpha(c)$, which controls the solvent solubility in the precipitate in this case, and k_{10} is the length of the [10] reciprocal-lattice vector of the precipitate in equilibrium. Here σ is the width corresponding to k_{10} .

An example phase diagram of a system with sample parameters in Eq. (46) is shown in Fig. 5. The metastable binodal (coexistence) and spinodal curves are shown below the coexistence curve.

E. Dynamics of precipitation: Results and discussion

We examined the precipitation process in a system that follows the XPFC model with density-density correlation function given by Eq. (46) and corresponding equilibrium phase diagram in Fig. 5. The situation examined corresponded to a quench to a temperature below the metastable spinodal curve. The spinodal curve marks an inflection point in the liquid free energy, meaning the metastable liquid becomes fully unstable and decomposes into regions of differing concentration as a result. A typical microstructure evolution sequence results for a typical quench of a uniform solution of $c = 0.3$ from the liquid phase to a temperature $T/T_0 = 0.07$ and is shown in Fig. 6. Frames (a)–(c) show the initial decomposition of the liquid, once below the spinodal temperature, into regions of high and low compositions. Frames (d)–(g) show that, once the concentration in the solute-rich regions of the decomposed liquid increases sufficiently, nucleation of the solid phase begins to occur in these confined liquid volumes. Once nucleated, the solid regions start and continue to grow at the expense of the liquid phase. This simulation is a typical example where the nucleation of precipitates is preceded by spinodal decomposition, which is consistent with the experimental findings mentioned above for the nanoparticle and calcium carbonate systems [15,28]. While one simulation sequence is shown here, this scenario was typical of all

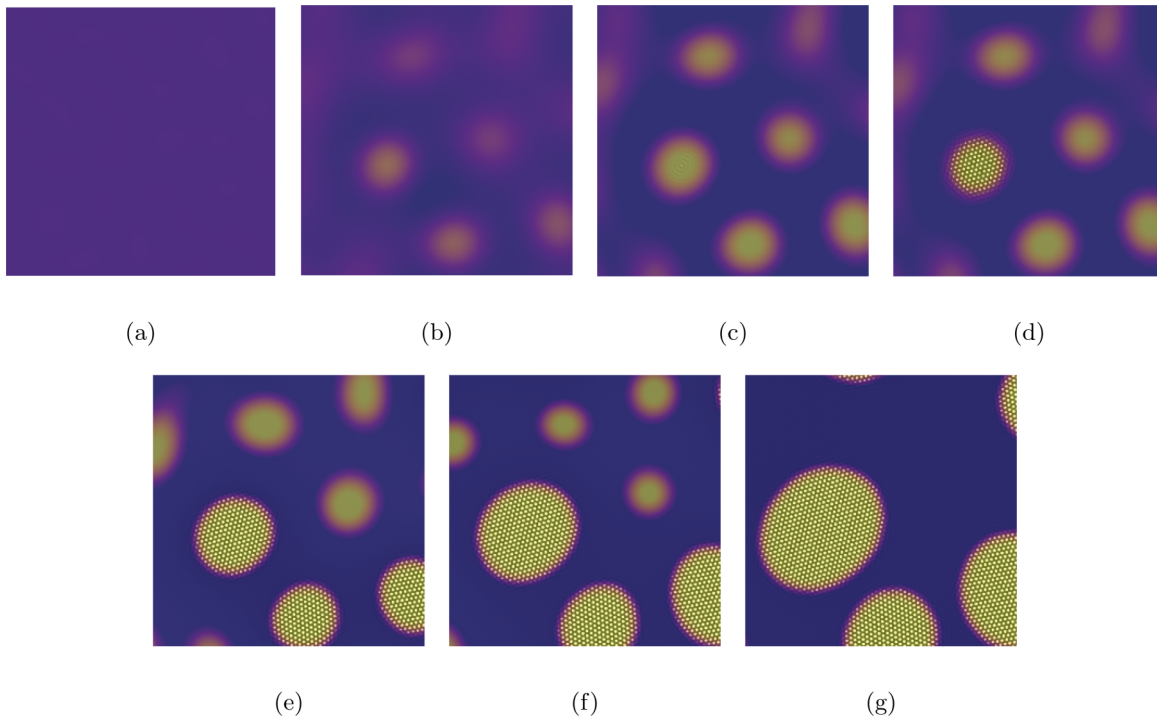


FIG. 6. Various stages of precipitation of nanoparticles from solution. All thermodynamic parameters are shared with Fig. 5. The initial condition is a uniform solution quenched abruptly to $T = 0.07$. The initial condition has average concentration $c = 0.3$, and the average relative density of the system is set to $n = 0.05$. Mobilities M_n and M_c are set to 1 and W_c is set to 3.0. Numerical parameters are grid spacing $\Delta x = 0.125$ on a 1024×1024 lattice with time-step size $\Delta t = 0.0025$. (a–d) Spinodal decomposition of the liquid and initial nucleation within solute-enriched liquid drops. (e, f) Further nucleation and solid growth at the expense of liquid regions.

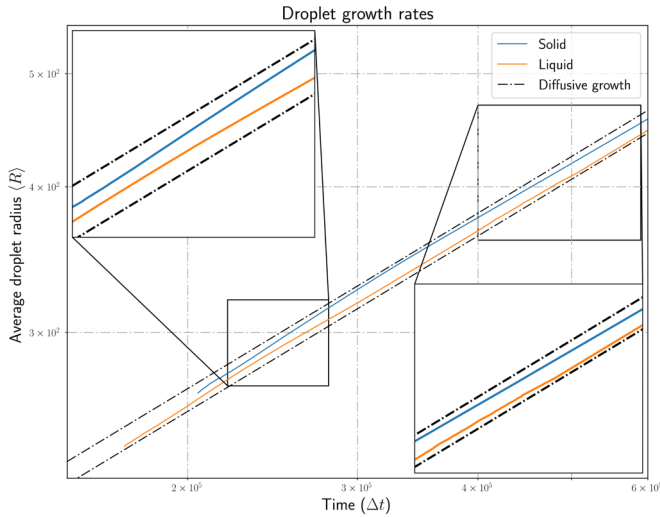


FIG. 7. Droplet growth $\langle R(t) \rangle$ vs time. Black line, $\sim t^{1/2}$ growth. Insets: Early hyperdiffusive growth of crystalline nanoparticles and late-stage hypodiffusive growth.

ensembles we ran and from which we gathered statistics for the data shown below.

As mentioned above, we observed that, once any solute-rich regions crystallize, their growth is accelerated at the expense of uncrystallized solute-rich liquid regions. We refer to this phenomena as *sacrificial growth* [Figs. 6(d)–6(f)]. To quantify the phenomena shown in Fig. 6, we examine the mean radius $\langle R(t) \rangle$ of solute-rich domains as a function of time, and average the results over an ensemble of 120 quenches analogous to those shown in Fig. 6. Here we define the mean radius of a crystal drop as the square root of its mean area:

$$\langle R(t) \rangle = \sqrt{\langle A(t) \rangle}. \quad (47)$$

The results obtained are not expected to depend on the precise definition of $R(t)$.

In purely diffusive growth the mean radius should scale as $\langle R(t) \rangle \sim t^{1/2}$, while at the late stages of growth, where coarsening occurs, the growth rate is expected to follow $\langle R(t) \rangle \sim t^{1/3}$ dynamics. In Fig. 7 we plot $\langle R(t) \rangle$ on a log-log graph. Lines corresponding to the diffusive growth exponent are also drawn for comparison to numerical results. The data show that for early times crystalline regions grow at a hyperdiffusive rate. This decays to hypodiffusive after uncrystallized regions have disappeared and coarsening takes over the kinetics of precipitation.

During the sacrificial growth period referred to above, we observe that nucleation is suppressed in the remaining uncrystallized, solute-rich, liquid regions. When both crystallized and uncrystallized solute-rich liquid drops exist, the solute is segregated into crystallized regions because of the difference in chemical potential. Constricted by surface tension and deprived of solute, these remaining droplets have a far slower nucleation rate (thermodynamic driving force) than when no crystallized regions existed. This can be seen more quantitatively by examining the fraction of uncrystallized liquid droplets versus time. This is shown in Fig. 8 for the case corresponding to the data in Fig. 6. At $\sim 50\%$ crystallization, we see a pronounced reduction in the nucleation rate as the

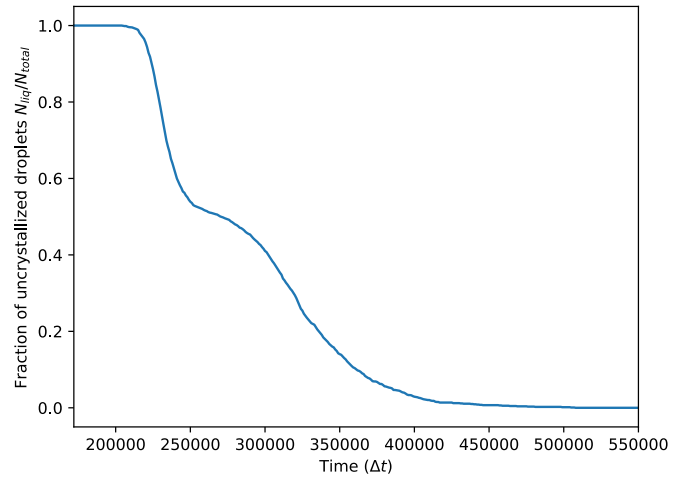


FIG. 8. Fraction of uncrystallized droplets vs time.

diffusive process of sacrificial growth dominates, consistent with our expected hypothesis above.

VIII. SUMMARY AND CONCLUSIONS

We have presented two generalizations of the binary XPFC model: the addition of an enthalpy of mixing and a general phenomenology for modeling density pair-correlation functions. Additionally, we have presented an application of this generalized model to the study of nonclassical precipitation pathways of nanoparticles.

We have shown that these generalizations are capable of modeling a broad class of binary alloys including syntectic and monotectic materials and can reproduce metastable components of material phase diagrams. Investigating the effects of elasticity on syntectic and monotectic materials is one future application.

Our application of the generalized model to nanoparticle precipitation describes the behavior of a quench followed by the multistep precipitation process of relevance to the precipitation of gold nanoparticles observed in recent experiments. It is noteworthy that the predicted results were done within a single framework and set parameters corresponding to the new XPFC alloy model introduced in this paper. The dynamical results shown here point to a richness in the landscape of kinetic pathways to precipitation. One direction for future application of the improved XPFC framework is to explore more of this landscape to help determine the effect of quench parameter and solution concentration in nucleation kinetics, as well as the polydispersity of precipitated particles, key features of interest to experimental investigations of this topic. Another area of application of the XPFC model introduced herein is the examination of elastic versus enthalpic effects during precipitation.

ACKNOWLEDGMENTS

The authors would like to acknowledge the financial support of the Canada Research Chairs Program and computational resources made available by Compute Canada and Calcul Quebec.

- [1] K. R. Elder, N. Provatas, J. Berry, P. Stefanovic, and M. Grant, *Phys. Rev. B* **75**, 064107 (2007).
- [2] K. Elder, K. Thornton, and J. Hoyt, *Philos. Mag.* **91**, 151 (2011).
- [3] G.-M. Lu, Y.-L. Lu, T.-T. Hu, and Z. Chen, *Comput. Mater. Sci.* **106**, 170 (2015).
- [4] M. Greenwood, C. Sinclair, and M. Militzer, *Acta Mater.* **60**, 5752 (2012).
- [5] V. Fallah, J. Stolle, N. Ofori-Opoku, S. Esmacili, and N. Provatas, *Phys. Rev. B* **86**, 134112 (2012).
- [6] V. Fallah, N. Ofori-Opoku, J. Stolle, N. Provatas, and S. Esmacili, *Acta Mater.* **61**, 3653 (2013).
- [7] V. Fallah, A. Korinek, N. Ofori-Opoku, N. Provatas, and S. Esmacili, *Acta Mater.* **61**, 6372 (2013).
- [8] N. Ganai, A. Saha, and S. Sengupta, *Eur. Phys. J. E* **36**, 1 (2013).
- [9] K. R. Elder and Z.-F. Huang, *J. Phys.: Condens. Matter* **22**, 364103 (2010).
- [10] Y. Lu, Y. Peng, and Z. Chen, *Superlattices Microstruct.* **97**, 132 (2016).
- [11] M. Seymour and N. Provatas, *Phys. Rev. B* **93**, 035447 (2016).
- [12] E. Alster, K. R. Elder, J. J. Hoyt, and P. W. Voorhees, *Phys. Rev. E* **95**, 022105 (2017).
- [13] M. Greenwood, N. Ofori-Opoku, J. Rottler, and N. Provatas, *Phys. Rev. B* **84**, 064104 (2011).
- [14] S. K. Mkhonta, K. R. Elder, and Z.-F. Huang, *Phys. Rev. Lett.* **111**, 035501 (2013).
- [15] N. D. Loh, S. Sen, M. Bosman, S. F. Tan, J. Zhong, C. A. Nijhuis, P. Král, P. Matsudaira, and U. Mirsaidov, *Nat. Chem.* **9**, 77 (2017).
- [16] N. Smith, Master's thesis, McGill University, Montreal, Canada, 2017.
- [17] The definition of ΔC in the original binary PFC model was expressed in different variables than those used here. However, expanding $\Delta c(r)$ here facilitates comparison with other theories.
- [18] J. Stolle and N. Provatas, *Comput. Mater. Sci.* **81**, 493 (2014).
- [19] S. Hu, Z. Chen, W. Xi, and Y.-Y. Peng, *J. Mater. Sci.* **52**, 5641 (2017).
- [20] The original model concentration was in fact a density difference, not true concentration.
- [21] M. Greenwood, N. Provatas, and J. Rottler, *Phys. Rev. Lett.* **105**, 045702 (2010).
- [22] The original XPFC works used a phenomenological prefactor $e^{-\sigma^2/C}$, where σ was considered a model temperature parameter and C was considered a constant. That choice was inspired by harmonic analysis in the solid phase and the Debye-Waller factor.
- [23] P. R. Subramanian and J. H. Perepezko, *J. Phase Equilib.* **14**, 62 (1993).
- [24] H. A. Murdoch and C. A. Schuh, *Acta Mater.* **61**, 2121 (2013).
- [25] J. Bezanson, S. Karpinski, V. B. Shah, and A. Edelman, *arXiv:1209.5145*.
- [26] N. Smith, Computer algebra system MAXIMA.JL, <https://github.com/nsmith5/Maxima.jl> (2017).
- [27] Computer algebra system MAXIMA, ver. 5.34.1 (2014).
- [28] A. F. Wallace, L. O. Hedges, A. Fernandez-Martinez, P. Raiteri, J. D. Gale, G. A. Waychunas, S. Whitelam, J. F. Banfield, and J. J. De Yoreo, *Science* **341**, 885 (2013).
- [29] R. J. Davey, S. L. M. Schroeder, and J. H. ter Horst, *Angew. Chem., Int. Ed.* **52**, 2166 (2013).
- [30] D. Gebauer and H. Cölfen, *Nano Today* **6**, 564 (2011).
- [31] D. Knezic, J. Zaccaro, and A. S. Myerson, *J. Phys. Chem. B* **108**, 10672 (2004).
- [32] J. F. Lutsko and M. A. Duran-Olivencia, *J. Phys.: Condens. Matter* **27**, 235101 (2015).
- [33] D. Erdemir, A. Y. Lee, and A. S. Myerson, *Acc. Chem. Res.* **42**, 621 (2009).